Advances in Water Resources 108 (2017) 205–215

Contents lists available at ScienceDirect

Advances in Water Resources

journal homepage: www.elsevier.com/locate/advwatres

Turbulent mixing and fluid transport within Florida Bay seagrass meadows

Jennifer C.R. Hansen, Matthew A. Reidenbach*

Department of Environmental Sciences, University of Virginia, Charlottesville, VA 22904, USA

ARTICLE INFO

Article history:
Received 12 November 2016
Revised 31 July 2017
Accepted 3 August 2017
Available online 9 August 2017

Keywords:
Seagrass
Turbulent kinetic energy
Mixing
Waves

ABSTRACT

Seagrasses serve an important function in the ecology of Florida Bay, providing critical nursery habitat and a food source for a variety of organisms. They also create significant benthic structure that induces drag, altering local hydrodynamics that can influence mixing and nutrient dynamics. *Thalassia testudinum* seagrass meadows were investigated to determine how shoot density and morphometrics alter local wave conditions, the generation of turbulence, and fluid exchange above and within the canopy. Sparsely vegetated and densely vegetated meadows were monitored, with shoot densities of 259 ± 26 and 484 ± 78 shoots m^{-2}, respectively. The temporal and spatial structure of velocity and turbulence were measured using acoustic Doppler velocimeters and an *in situ* particle image velocimetry (PIV) system positioned both above and within the seagrass canopy. The retention of fluid within the canopy was determined by examining *e*-folding times calculated from the concentration curves of dye plumes released within the seagrass canopy. Results show that a shear layer with an inflection point develops at the top of the seagrass canopy, which generates instabilities that impart turbulence into the seagrass meadow. Compared to the overlying water column, turbulence was enhanced within the sparse canopy due to flow interaction with the seagrass blades, but reduced within the dense canopy. Wave generated oscillatory motion penetrated deeper into the canopy than unidirectional currents, enhancing fluid exchange. Both shoot density and the relative magnitude of wave- versus current-driven flow conditions were found to be important controls on turbulent exchange of water masses across the canopy-water interface.

1. Introduction

Significant aboveground biomass is created by seagrass meadows, which serves as an obstruction to flow, altering local hydrodynamics that influence the meadow's productivity (Carr et al., 2016; Peralta et al., 2006; Schanz and Asmus, 2003), photosynthetic rates (Koch, 1994; Rheuban et al., 2014), nutrient uptake (Cornelisen and Thomas, 2009; Thomas et al., 2000), and sediment dynamics (Bouma et al., 2009; Hansen and Reidenbach, 2013; Koch, 1999). Aquatic plant communities rely on the delivery of nutrients from the surrounding water column (Lei and Nepf, 2016; Taylor et al., 1995), which must cross the canopy-water interface. This is particularly important in meadows such as those present in Florida Bay, where uptake of nutrients occurs near the mass-transfer limit (Cornelisen and Thomas, 2009).

The seagrass canopy imparts significant fluid drag, which reduces fluid velocities within the canopy (Adhitya et al., 2014; Ghisalberti and Nepf, 2004; Hansen and Reidenbach, 2012), and, as found in current-driven flows, creates a shear layer at the canopy-water interface (Nepf, 2012a). These shear layers develop to a finite thickness (Ghisalberti and Nepf, 2002) effectively separating the canopy into two regions (Nepf et al., 2007). Near the canopy-water interface exchange is driven by turbulent transport generated by flow instabilities (Ghisalberti and Nepf, 2004; Lacy and Wyllie-Echeverria, 2011). Deeper within the canopy, a region of limited transport exists where stem-generated turbulence controls exchange processes (Nepf et al., 2007). In the upper region, transport occurs through the development of Kelvin–Helmholtz vortices created by the velocity profile instability (Raupach et al., 1996). These eddy structures not only carry momentum across the canopy-water interface, but also promote the exchange of dissolved gasses and nutrients (Cornelisen and Thomas, 2004; Long et al., 2015; Weitzman et al., 2013).

The density of the seagrass meadow will also influence the turbulence and shear layer structure (Adams et al., 2016). As seagrass density increases, turbulent energy generated by the Kelvin–Helmholtz vortices in the shear layer is lost more rapidly, shortening the penetration depth of turbulence into the canopy (Ghisalberti and Nepf, 2004). These dense canopies resemble mixing layers (Cornelisen and Thomas, 2009), formed when velocities

* Corresponding author.
E-mail address: reidenbach@virginia.edu (M.A. Reidenbach).

http://dx.doi.org/10.1016/j.advwatres.2017.08.001
0309-1708/

in two adjacent regions flow at different speeds, and are separated by a shear region containing an inflection point (Raupach et al., 1996). Typically, within vegetated flows, turbulence below the mixing layer is quickly damped and becomes negligible within the canopy (Finnigan, 2000; Lacy and Wyllie-Echeverria, 2011). Within sparsely vegetated canopies shear layers may not form and velocity profiles can be logarithmic (Nepf, 2012a), or the flow may resemble disturbed boundary layers where turbulence is enhanced (Hansen and Reidenbach, 2013; Lacy and Wyllie-Echeverria, 2011; Lawson et al., 2012) within the canopy due to stem-wake interactions with individual seagrass blades.

In coastal environments, many seagrass canopies are exposed to wind-generated waves in addition to tidally-dominated currents. In the presence of waves, oscillatory motion leads to movement of the seagrass blades, enhancing fluid exchange (Koch and Gust, 1999; Pujol et al., 2013) and nutrient uptake (Weitzman et al., 2013) across a wide range of seagrass densities. Within flexible canopies, high frequency oscillatory flows have been found to be damped more rapidly than low frequencies as waves propagate across the meadow (Bradley and Houser, 2009), while low frequency waves have also been found to more effectively penetrate into the meadow (Hansen and Reidenbach, 2012). However, across rigid canopy-water interfaces, the reduction in wave orbital velocities, and thus wave energy, was found to be greater for lower wave frequencies (Lowe et al., 2007), suggesting complex dynamics dependent on the canopy type and range of wave frequencies under consideration. Waves, in general, increase within-canopy water velocities and turbulence (Fonseca, 1983; Hansen and Reidenbach, 2013; Koch and Gust, 1999; Luhar et al., 2013; Widdows et al., 2008), leading to greater mixing and increased mass transfer (Lowe et al., 2005a,b). As shoot density increases, increases in mass transfer become more pronounced relative to unidirectional flows (Lowe et al., 2005b; Weitzman et al., 2013).

This study aims to investigate the structure of flow and turbulent mixing within and above seagrass canopies by quantifying water velocities and the development of turbulence in relation to the seagrass shoot density across two *Thalassia testudinum* seagrass canopies in Florida Bay. The specific questions this study addresses are: 1. How do changes in *T. testudinum* seagrass blade density and morphology alter local wave conditions, fluid shear, and turbulence both above and within the canopy and 2. How do these flow-structure interactions alter the exchange of fluid between the canopy and overlying water column? To further illuminate the influence of the seagrass structure on local hydrodynamics, velocity and turbulence measurements were then compared to an unvegetated site. The novelty of this study is in coupling high temporal-resolution measurements using acoustic Doppler velocimeters (ADV) with detailed spatial measurements using a novel *in situ* particle image velocimetry (PIV) system.

2. Methods

2.1. Study area

Florida Bay is characterized as a shallow basin, which is separated from the Atlantic Ocean by the Florida Keys to the east and the Gulf of Mexico to the west. The study area was within the Everglades National Park, which has an area of 1800 km^2 with 1660 km^2 of seagrass; with *Thalassia testudinum* being the major species of seagrass in the region (Zieman et al., 1989). Three locations within Florida Bay were chosen as study sites, two seagrass sites of different seagrass shoot densities, and an unvegetated site to serve as a comparison for local flow conditions in the absence of considerable benthic structure (Fig. 1). The northeast portion of Florida Bay tends to have sparse, patchy *T. testudinum* seagrass beds, while further south mixed beds of *T. testudinum* and *Halodule wrightii* are present. The unvegetated site and the sparsely vegetated *T. testudinum* seagrass sites were 0.2 km apart, with the dense mixed *T. testudinum* and *H. wrightii* seagrass site located 29.8 km to the southwest. Within the mixed bed, *T. testudinum* shoot density was approximately double that of *H. wrightii*. Further, the projected frontal area per unit plan area (defined as ah, where $a = d/\Delta S^2$, d is blade width, ΔS is the spacing between seagrass blades, and h is the canopy height (Nepf and Vivoni, 2000) of *H. wrightii* in this study was only 2.3% of that provided by *T. testudinum* where they co-exist, and therefore the impact of *H. wrightii* on the flow dynamics is expected to be minimal. Shoot densities reported in this study represent that of *T. testudinum* only. Experiments at each site were conducted during consecutive weeks in September 2009.

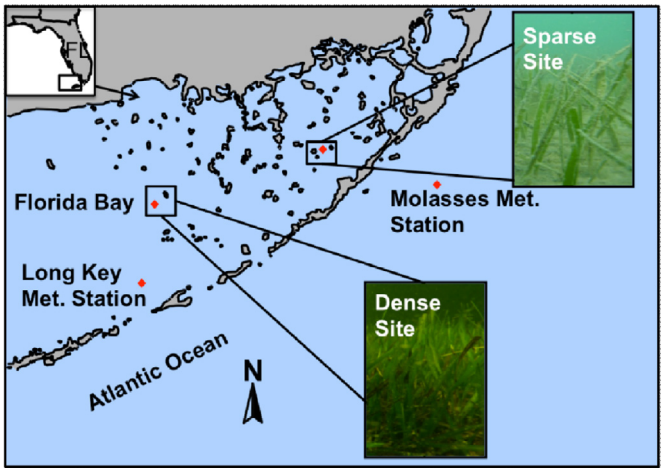

Fig. 1. Study sites, located in Everglades National Park, near Bottle Key and within Rabbit Key Basin in Florida Bay, FL, USA. Two separate *T. testudinum* meadows, labeled Sparse Site and Dense Site are located 29.8 km apart. An additional unvegetated site (0.2 km from the sparse site) as a comparison to flows in the absence of benthic structure, was also monitored. Wind data was obtained from two National Oceanographic and Atmospheric Administration (NOAA) data buoy meteorological stations, labeled Long Key Met. Station and Molasses Met. Station.

2.2. Seagrass morphometrics

Seagrass density was measured *in situ* at each site by counting the number of seagrass shoots per 0.25 m^2 quadrat randomly placed on the seafloor (Table 1). Seagrass blade length, blade width, and canopy height were measured via image analysis of the canopy with ImageJ® software from 5 separate images randomly taken within the meadow. Images of the seagrass meadow were taken in profile with a reference bar for scale. In the image-processing suite, the pixel length of each measurement was scaled with the reference length in the image. This methodology was confirmed and used in *Zostera marina* meadows in Virginia (Hansen and Reidenbach, 2013) where image-analysis of the meadows was compared to morphometric analysis of seagrass shoots sampled from the field and measured in the lab. Canopy height, defined as the average of the longest 2/3 of the blade lengths (Koch et al., 2006), were 15.2 ± 2.0 cm and 37 ± 4.8 cm at the sparse and dense sites, respectively (Table 1). This compares to the significantly different average blade lengths of 14 ± 2 cm and 33 ± 7 cm between the two locations (one-way ANOVA, $p < 0.05$). The seagrass meadows had significantly different mean densities, 259 ± 26 shoots m^{-2} (median value of 260 shoots m^{-2}) and 484 ± 78 shoots m^{-2} (median value of 500 shoots m^{-2}, one-way ANOVA, $p < 0.05$; Table 1), and are therefore referred to as the sparse and dense seagrass sites to represent their relative shoot densities. The dense site is on the lower range of that present within Florida Bay; average shoot density across the Bay in 1994 was 565.7 ± 50.5 (±SE)

Table 1
Thalassia testudinum. Morphometrics of seagrass meadows at two locations in Florida Bay, FL. Seagrass density was measured using *in situ* 0.25 m^2 quadrat shoot counts. Canopy height was calculated as the average of the longest 2/3 of the blade lengths measured. Blade width was measured at the midpoint along the length of the blade. Values represent averages ± standard deviations with *n* values representing the number of samples in each average.

	Canopy height (cm)	*n*	Density (shoots m^{-2})	*n*	Blade width (cm)	*n*
Sparse	15.2 ± 2.0	66	259 ± 26	10	0.74 ± 0.27	50
Dense	37 ± 4.8	50	484 ± 78	10	0.80 ± 0.19	40

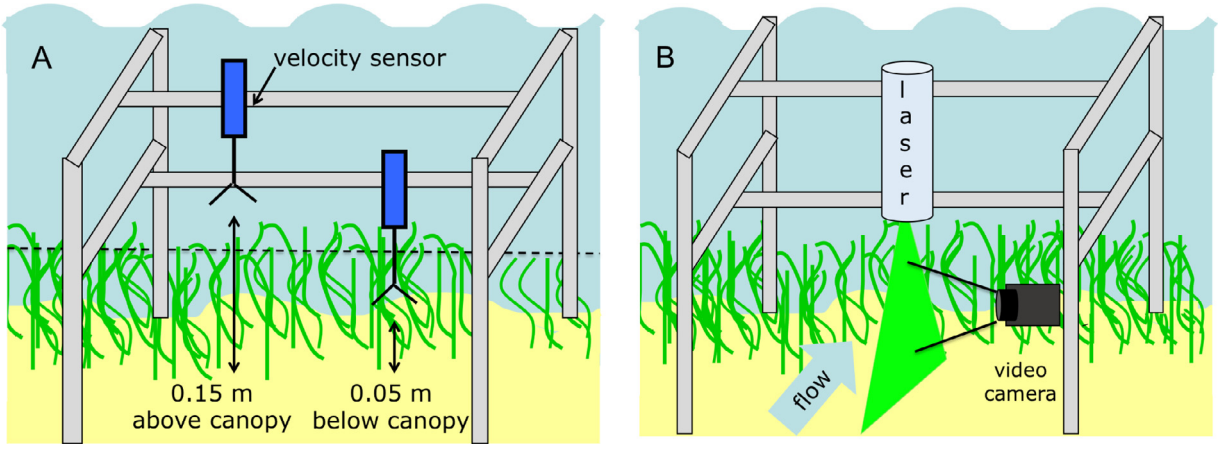

Fig. 2. Instrument setup for measurements of velocities above and within the seagrass canopy. **A** Acoustic Doppler Velocimeters arranged to measure velocities above and within the seagrass canopy. Dotted line indicates top of the canopy. **B** Particle image velocimetry system consisting of a digital camera and laser within a waterproof housing.

(Hall et al., 1999), between 1989 and 1995 shoot density was between 518 ± 49 and 768 ± 33 (±SE) (Zieman et al., 1989), and in 2005 it was reported to range from 665 ± 139 to 1533 ± 137 (Borum et al., 2005).

2.3. Instrumentation

Water velocities were measured using two Nortek Vector© acoustic Doppler velocimeters (ADVs), with a 1 cm^3 sampling volume located at $z = 0.35$ m and $z = 0.15$ m above the seafloor at the unvegetated site, $z = 0.3$ m and $z = 0.1$ m above the seafloor ($z/h = 2.0$ and 0.7, where h is canopy height) at the sparse seagrass site, and $z = 0.5$ m and $z = 0.3$ m above the seafloor ($z/h = 1.4$ and 0.8) at the dense seagrass site (Fig. 2). These elevations ensured that when seagrass was present, the sample volumes were consistently positioned 0.15 m above and 0.05 m below the canopy, respectively. Simultaneous velocity and pressure were recorded at 32 Hz for 10 min bursts every 20 min over a 72 h period in order to obtain high-resolution temporal data. This 10 min time interval was chosen as the best balance between convergence of mean statistics, while minimizing drift due to changes in flow conditions (Gross and Nowell, 1983). Data were rotated from earth coordinates, East, North, and Up, to the dominant horizontal flow direction, u, minimizing the transverse direction, v, and leaving the vertical, w, unchanged. The rotation was defined by resolving the angle between the two horizontal velocity vectors on mean values from each 10 min interval and applying the rotation matrix to the corresponding instantaneous values. Velocity values with low signal to noise ratios were removed, which occurred due to interference with the sensor head from drifting wrack or from fish swimming below the sensors. Wind data was obtained from the National Data Buoy Center C-MAN stations at Molasses Reef, FL (MLRF1) and Long Key, FL (LONF1), as marked in Fig. 1. Wind direction and magnitude were reported once every 10 min for each site.

Fine-scale spatial measurements of turbulence and shear layer structure were obtained using an underwater particle image velocimetry (PIV) system (Stocking et al., 2016). With this technique, short snapshots of two-dimensional velocity can be obtained with high spatial resolution over a narrow depth range around the canopy-water interface. The system includes a 532 nm, 300 mW laser (Laserglow Technologies), mounted in a custom-built underwater housing, which contained a 20° convex lens (CVI-Melles Griot) to create a laser light sheet 0.2 cm thick by 20 cm wide (Fig. 2). This light sheet illuminated suspended particles within the flow and a high definition camera (Sony HDR-HC7), was used to image particles. The camera was equipped with a 530 ± 10 nm bandpass filter (Omega Optical 530BP10) to remove ambient light such that the PIV system could be operated during daylight conditions. Particle motion was recorded by the video camera over a 12 cm by 6 cm viewing window at 30 frames per second. Ideal particle seeding concentration for achieving high accuracy (~ 1%) typically ranges from about 5–10 particles per 32 × 32 pixel interrogation subwindow (Cowen and Monismith, 1997; Raffel et al., 1998). If natural abundances of suspended particles were not of sufficient quantity, the water was seeded upstream with neutrally buoyant 100 µm clay particles. Due to the planar nature of the PIV measurements, the laser sheet was aligned to the dominant direction of flow.

2.4. Data analysis

PIV videos were first converted to a sequence of individual images, then sequential image pairs were processed using a cross-correlation analysis to track particle motions over time using MatPIV, a PIV analysis software program written for Matlab® (Sveen and Cowen, 2004). Each image pair is first analyzed on a 32 × 32 pixel interrogation subwindow with 50% overlap, with subsequent refinement of the window size, such that the final resolution of horizontal, u, and vertical, w, velocities is on a 16 × 16 pixel scale. Previous investigations determined the accuracy of the PIV measurements to be $\pm 6\%\bar{u}$, where $\bar{u}$ is the mean velocity (Reidenbach et al., 2008).

Currents, wave orbital velocities, and turbulent fluctuations are resolved using both ADV and PIV instrumentation. A longer temporal data set was obtained with the ADVs but was limited to only two single-point locations in the water column, while the PIV instrument is limited to a short time-series bursts (≈1–2 min) but yields detailed spatial data at the canopy-water interface. Therefore, flow parameters were calculated in similar ways but represent either more detailed temporal or spatial resolution.

When waves and currents are both present, velocity fluctuations are associated with both waves and turbulence, and a wave-turbulence decomposition must be performed (Trowbridge, 1998). Often, a spectral decomposition of the wave and turbulence field, called the Phase method, is employed to separate turbulence from waves (Bricker and Monismith, 2007; Hansen and Reidenbach, 2012), which relies solely on the use of high-frequency measurements of the three components of velocity. However, this method may be prone to errors if wave orbital velocities are large relative to mean currents (Bricker and Monismith, 2007). An alternative method, first derived by Benilov and Filyushkin (1970), can be employed when wave motions are large relative to mean currents. In this method, water velocities that correlate with the displacement of the free surface are considered to be due to waves, and those that do not correlate are due to turbulence. In practice, this method requires the simultaneous measurements of velocity and free-surface position, either from a pressure or capacitance type wave gauge (Bricker and Monismith, 2007). This method can be applied to ADV measurements due to the simultaneous high-frequency measurements of velocity and pressure.

Instantaneous horizontal and vertical velocities can be written as:

$$u = \bar{u} + u' + \tilde{u} \qquad w = \bar{w} + w' + \tilde{w} \tag{1}$$

where $\bar{u}$, $\bar{w}$ are the temporal mean velocities, u', w' are velocity fluctuations due to turbulence, and $\tilde{u}$, $\tilde{w}$ are velocities due to orbital wave motions. Turbulent stresses are found by first calculating the spectrum of the raw stresses from the *u, v,* and *w* velocities. The cross-spectrum is then computed from the cross correlation of each component of velocity with the pressure signal. The assumption that turbulence is uncorrelated with the pressure variation caused by the displacement of the free surface dictates that all but the wave correlated motions go to zero. Mathematically, the wave stress can then be calculated through the spectral sum:

$$\overline{\tilde{u}\tilde{w}} = \int_{-f_{Nyquist}}^{f_{Nyquist}} S_{\tilde{u}\tilde{w}}(f)d(f) \tag{2}$$

where $S_{\tilde{u}\tilde{w}}(f)$ is the two-sided cross-spectral density of the wave-induced orbital velocities and f is the frequency. $S_{uw}(f)$ is computed from the full spectrum and integrated in a similar manner as Eq. (2) to quantify $\overline{uw}$. The turbulent Reynolds stress can then be found as the difference between the total stress and the wave stress after integration:

$$\overline{u'w'} = \overline{uw} - \overline{\tilde{u}\tilde{w}} \tag{3}$$

This technique, and its application to water waves, is described more fully in Bricker (2003) and Bricker and Monismith (2007).

Utilizing this method, mean values of the turbulent Reynolds stress, $\overline{u'w'}$, are computed over each 10 min sampling window. Although components of the turbulent kinetic energy (TKE), $\overline{u'u'}$, $\overline{v'v'}$, and $\overline{w'w'}$ can also be computed using the same technique, they are prone to produce large errors due to squared terms of the individual components of the velocity fluctuations. Therefore, TKE values are not reported. PIV measurements contain no pressure or free surface displacement information, therefore PIV data cannot be used to compute Reynolds stresses or TKE utilizing the Benilov and Filyushkin (1970) method.

2.5. Dye tracer studies

To obtain a qualitative understanding of fluid retention times within and above the seagrass meadow, Rhodamine WT dye was released at depths equivalent to the sampling volumes of the two ADVs at each of the three study sites. Dye was released in a finite pulse from a 5 mL syringe and water samples were then obtained an average of 6 m downstream. The downstream location was chosen based on the dominant current direction, initially located by observing the progression of a tracer released into the flow. At 30 s intervals, water samples were taken from this static downstream location and dye concentrations were measured with a Turner Designs AquaFluor handheld fluorometer. Multiple concentration curves were obtained at various locations within the seagrass and bare sites. Downstream concentrations, C, were normalized by the dye concentration at release, C_o. The e-folding time was then calculated as the time for the peak in normalized dye concentration, C/C_o, to reduce to $\frac{1}{e}C/C_o$ (Abdelrhman, 2002).

Residence times are defined as the retention of a water-mass within a set boundary, representing a finite transport through a system (Monsen et al., 2002). Dye tracers within a canopy can be used to quantify this residence time and reflect the relative rate of exchange of water from within to outside the canopy (Nishihara et al., 2011). This metric is spatially variable and represents a local measure (Monsen et al., 2002) of the relative time water masses are in contact with the seagrass.

3. Results

3.1. Site characterization

Physical characteristics of each site are reported in Fig. 3. Prevailing wind direction during the deployment at the bare site was toward the southwest, while winds during the sparse and dense deployments were toward the northwest (Fig. 3A). The fetch length at each of the sites was statistically similar (one-way ANOVA on fetch lengths at 30° intervals, $p = 0.9$); therefore wave development (Fig. 3B) was primarily dependent on wind magnitude. Water temperature was consistent throughout the deployment period, with temperature ranges of 29–31 °C.

Average water column depths (± tidal amplitude) were 2.6 ± 0.04, 2.5 ± 0.03, and 2.7 ± 0.10 m at the bare, sparse, and dense sites, respectively (Fig. 3C). Water flow within the Northeastern portion of Florida Bay is restricted from the tidal influences of the neighboring Atlantic Ocean and the Gulf of Mexico by the numerous keys and shallow banks (Wang et al., 1994); therefore, in this area wind driven currents dominate (Holmquist et al., 1989). Thus, both the bare and sparse sites had small tidal amplitudes. The dense seagrass site was more influenced by tides from the Atlantic Ocean, resulting in significantly greater tidal amplitudes (one-way ANOVA with Bonferroni multi-comparison, $p < 0.05$) and faster water currents compared to the unvegetated or sparse seagrass sites (Fig. 3D).

3.2. Velocity structure

Above and within canopy mean horizontal velocities, $\bar{u}$, at the two seagrass sites were determined from ADV measurements and compared to the unvegetated site. Within canopy velocities were reduced 45% and 54% at the sparse and dense site, respectively, compared to above the canopy. Although the seagrass measurements were taken at higher locations in the water column due to the presence of seagrass, these reductions were significantly greater (one-way ANOVA with Bonferroni multi-comparison, $p < 0.05$) than the 26% reduction in near-bed flows at the bare site (Fig. 4).

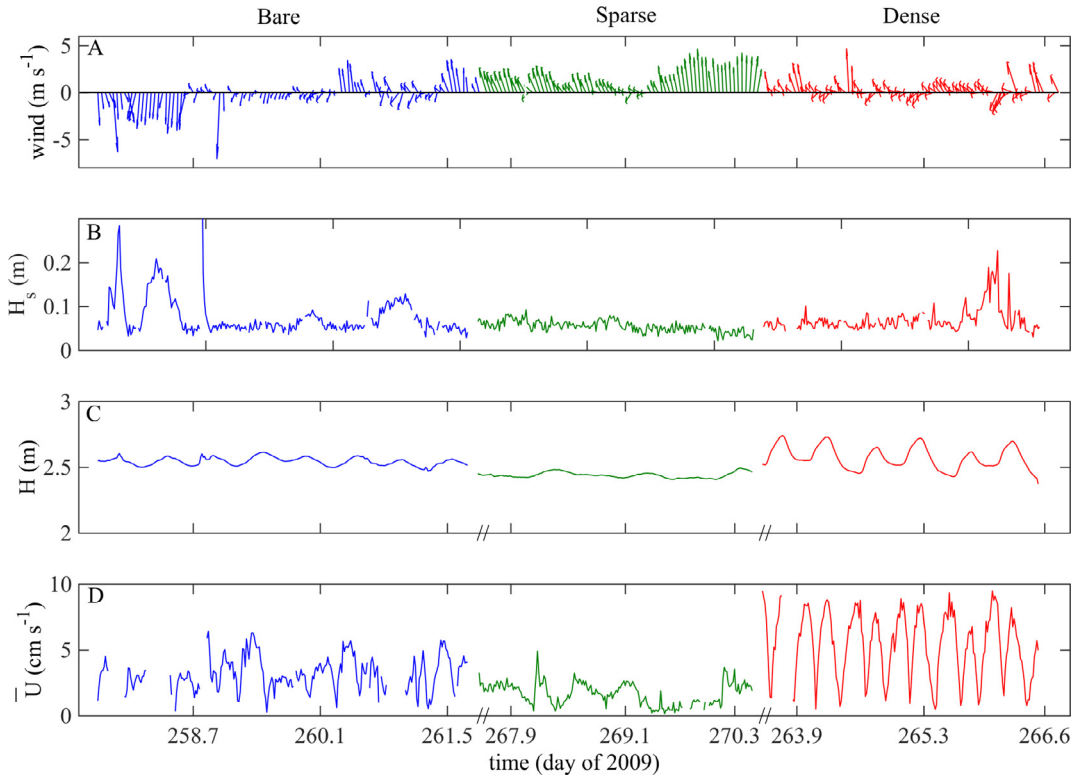

Fig. 3. Physical parameters at the unvegetated (bare), sparse seagrass, and dense seagrass sites. Note discontinuous time record between successive monitoring of the sites. **A** Wind magnitude and direction, arrows denote the direction toward which the wind is blowing with Northward up and Eastward to the right, **B** significant wave height, H_s **C** water depth (H), and **D** horizontally averaged current, $\bar{U} = \sqrt{\bar{u}^2 + \bar{v}^2}$, above the seagrass meadow.

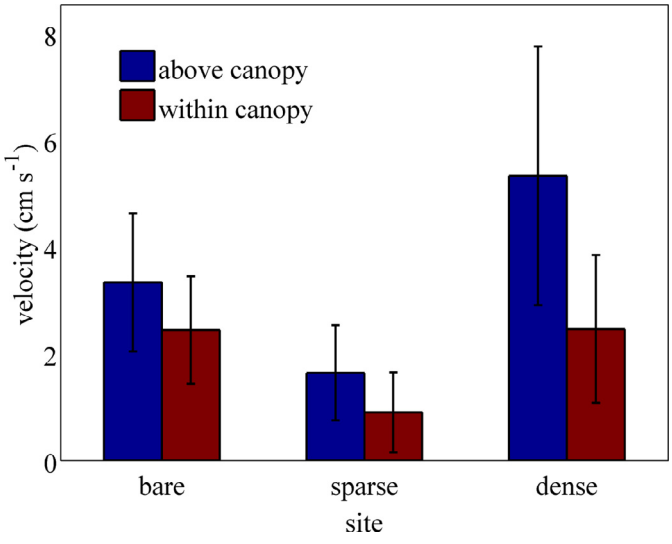

Fig. 4. Mean velocities, $\bar{u}$, (± 1 s.d.) above and within the seagrass meadow at the bare, sparse seagrass, and dense seagrass meadows. Measurements were located at $z = 0.35$ m and $z = 0.15$ m above the bed at the unvegetated site, $z = 0.3$ m and $z = 0.1$ m above the bed ($z/h = 2.0$ and 0.7, where h is canopy height) at the sparse seagrass site, and $z = 0.5$ m and $z = 0.3$ m above the bed ($z/h = 1.4$ and 0.8) at the dense seagrass site.

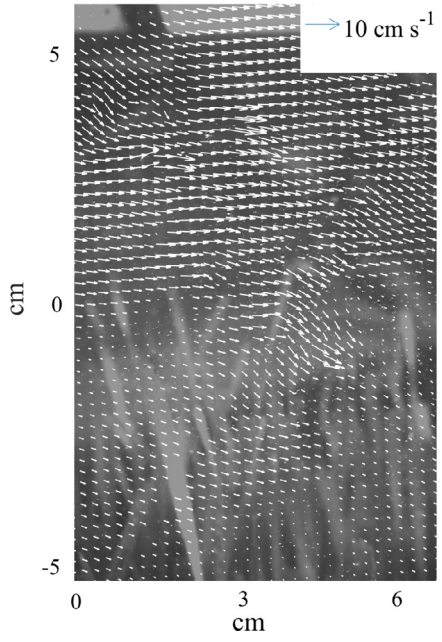

Fig. 5. PIV image of instantaneous velocity structure at the dense seagrass site, showing the strong shear layer and instabilities that form at the top of the canopy. Top of the canopy is located at $z = 0$ cm.

Fine scale velocity profiles, measured at 2 mm spatial resolution across the top of the seagrass canopy, were obtained from particle image velocimetry (PIV). At the sparse site, unidirectional flows showed low shear above the canopy but a shear layer developed near the top of the canopy. At both the sparse and dense sites, flow was reduced within the seagrass canopy compared to above, but stronger mean velocity shear developed within the dense canopy (Fig. 5). Shear layers developed due to the presence of the seagrass structure, which included an inflection point of instability at the canopy-water interface. Vertical profiles of velocity were normalized by the maximum mean horizontal velocity at the top of the profile, U_0. Normalized profiles show enhanced flow pene-

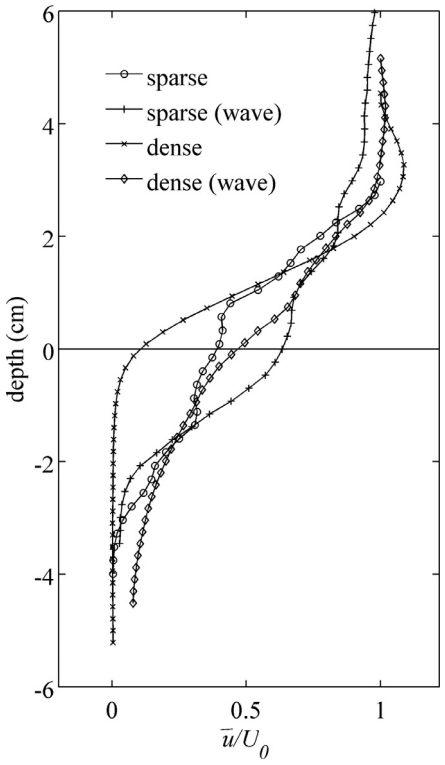

Fig. 6. Velocity profiles for current- and wave-dominated flow conditions at the sparse and dense seagrass sites normalized by the temporally averaged horizontal velocity at the top of each profile, U_0. Horizontal line at depth = 0 cm represents the top of the seagrass canopy during non-wave conditions. Mean estimates, $\bar{u}$, were formed by first averaging the horizontal component of velocity, u, temporally then horizontally across all the PIV velocity vectors to collapse the spatial velocity data to a vertical profile.

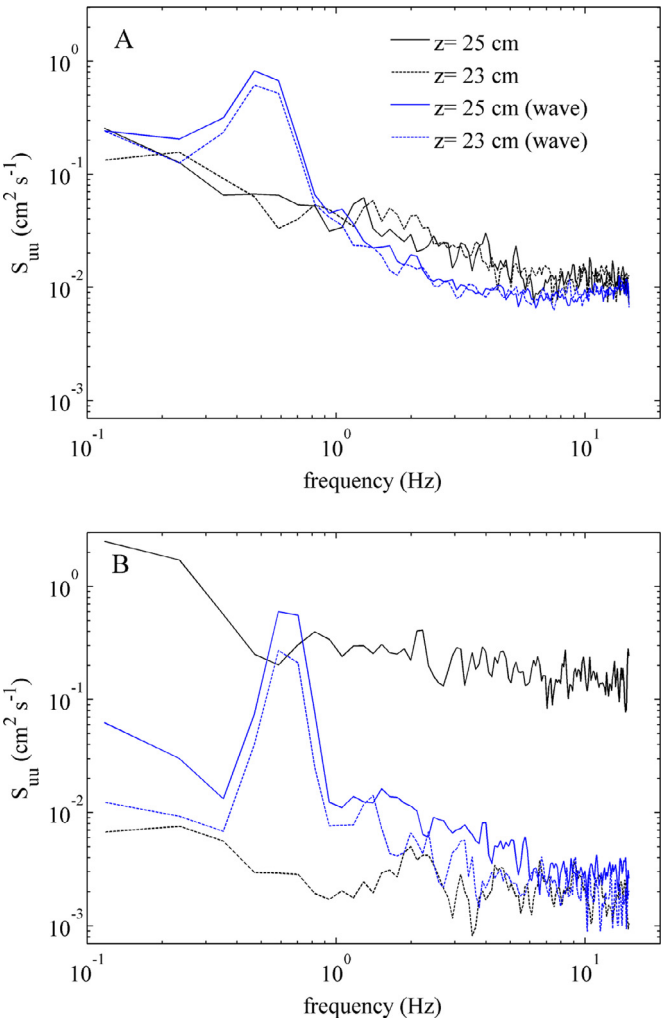

Fig. 7. Velocity spectra obtained via PIV for current- and wave-dominated flow periods (black and blue lines, respectively) at two locations in the mid-water column for the **A** bare site and the **B** dense seagrass site, At the bare site, locations correspond to an elevation of $z = 25$ cm and $z = 23$ cm above the seafloor. This corresponds to the same change in elevation across the seagrass canopy at the dense seagrass site, where the upper sampling location was 1 cm above the top of the seagrass canopy and the lower sampling location was 1 cm below the top of the canopy.

tration into the sparse meadow as compared to the dense meadow for current-dominated flows (Fig. 6). At the bare site, the mean-flow profile through the water column indicated the presence of a logarithmic distribution in the velocity profile (not shown) and low velocity shear ($d\bar{u}/dz$) as compared to the vegetated canopies. For wave-dominated flow conditions, the strength of the velocity shear decreased and the thickness of the shear region increases. During these periods, wave dominated flows produced higher velocity magnitudes (normalized by velocity above the canopy) within the meadow than under current-dominated flows. This enhancement of penetration of wave-dominated flow in to the canopy was greater for the dense canopy than the sparse canopy.

3.3. Velocity spectra and wave orbital motion

Power spectral densities (PSDs) of horizontal velocities during current- and wave-dominated flow conditions were determined using PIV data, and spectra from above and within the seagrass canopy were compared to the bare site (Fig. 7). At the bare site, the two spectra shown for the current-dominated flow condition (black lines) are similar, suggesting that the magnitude of turbulence and its structure is similar (Fig. 7A). For the wave-dominated condition (blue lines), the energy within the wave band decreased slightly with depth, as expected by linear wave theory. At the dense canopy, there is again a similar slight reduction in turbulent energy within the wave peak of the spectrum (blue lines), but a large decrease in turbulent energy across the spectra for unidirectional flow conditions (black lines, Fig. 7B). Typically, a −5/3 slope region only forms when there is a well-defined inertial subrange, and we have found this is the case when mean flows exceed 5–10 cm s^{-1}. These spectra suggest that the flow is dominated by turbulence and that a typical cascade from large to small turbulent eddies does not form. This is indicative of both a low energy environment and one where turbulent eddies are being formed across a range of scales, likely due to a combination of shear and wake generated turbulence. The reduction of total energy from above to within the canopy indicates that velocities do not penetrate into the canopy. When waves were present, the spectral energy within the wave-band of the velocity spectrum accounted for an average of 55 ± 14% of the total energy within the sparse site and 62 ± 10% within the dense seagrass site.

To determine the extent to which reduction of wave orbital velocities within the seagrass canopy are due to natural attenuation with depth versus interaction with the seagrass blades, estimates of wave-orbital velocities were computed using pressure sensor measurements from the ADV (u_{om}) and compared with orbital velocities computed through velocity spectra (u_{os}). Horizontal orbital velocity using velocity spectra is calculated as (Wiberg and Sherwood, 2008):

$$u_{os} = \sqrt{2 \sum_j S_{\tilde{u}\tilde{u}_j} \Delta f_j} \tag{4}$$

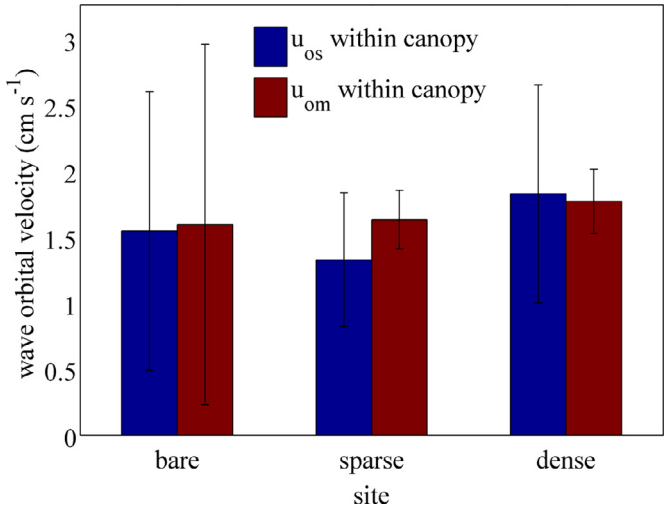

Fig. 8. Horizontal wave orbital velocities, u_{os}, within the seagrass meadows and at the bare site from spectral analysis, as well as expected orbital velocities, u_{om}, calculated via linear wave theory. Error bars represent ±1 s.d.

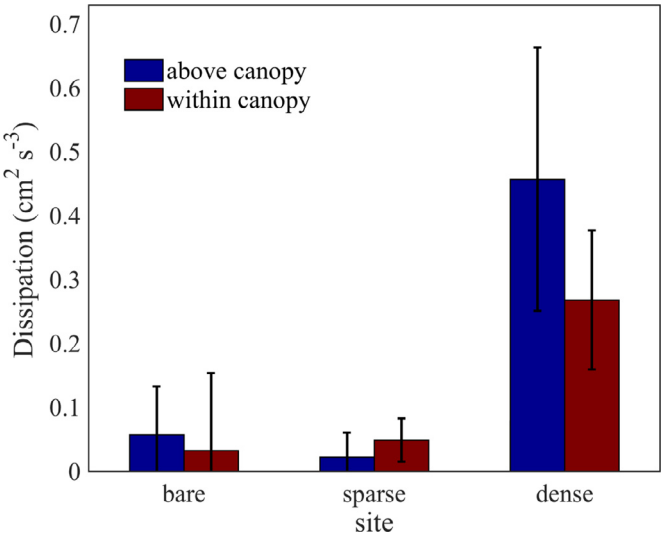

Fig. 9. Turbulent dissipation rate (ε ±1 s.d.) at the bare, sparse, and dense seagrass sites.

where u_{os} is the root-mean-squared (rms) orbital velocity, $S_{\tilde{u}\tilde{u}}$ is the wave portion of the horizontal velocity spectra, and f is the frequency. This formulation computes the significant orbital velocity, or the orbital velocity produced from the significant wave height, which has traditionally been defined as the average height of the highest one-third of waves during a sampling interval (Wiberg and Sherwood, 2008). This method directly quantifies wave motion within the seagrass bed. Utilizing pressure measurements from above the seagrass canopy and linear wave theory for small amplitude waves, the horizontal component of orbital velocity, u_{om}, at any z location within the water column can be estimated as (Dean and Dalrymple, 1991):

$$u_{om} = \frac{\pi H_s \cosh(kz)}{T \sinh(kH)} \tag{5}$$

where H_s is the significant wave height, T is wave period, z is the location above the seafloor, H is the water column depth, and k is the wave number such that $k = 2\pi/L$ where L is the wavelength. The wavelength, L, was calculated as: $L = L_\infty \sqrt{\tanh(\frac{2\pi H}{L_\infty})}$, where $L_\infty = \frac{g}{2\pi} T^2$. u_{om} was then estimated for the same z location above the bed as that computed for u_{os}.

The spectral method utilizes direct measures of water motion to compute orbital wave velocities, while linear wave theory utilizes pressure variations driven by sea surface displacements and assumes the bed is frictionless to compute orbital motions. Therefore, differences between orbital velocities computed from the spectral and linear wave theory estimates should indicate the relative dampening of wave velocity due to frictional interaction with the seagrass canopy. At all sites, there is a small, though not statistically different, variance in the magnitude of orbital velocity computed from linear wave theory, u_{om}, as compared to the spectral method, u_{os} (one-way ANOVA, $p > 0.05$). This suggests that, at the seagrass densities measured within this study, they do not have a significant impact on the local attenuation of wave orbital motion within the canopy (Fig. 8).

3.4. Turbulent dissipation rates

Turbulent dissipation rates, ε, were calculated from the one-dimensional spectrum of vertical velocities, as described in Reidenbach et al. (2006). Briefly, a line of best fit with a −5/3 slope was applied to the intertial subrange of the spectum during time periods without a substantial wave signal, and the magnitude of the interpolated power density was used to solve for turbulent dissipation according to the equation:

$$S_{ww} = \frac{12}{55} \frac{1}{|\bar{u}^{2/3}|} \alpha \varepsilon^{2/3} k^{-5/3} + n \tag{6}$$

where S_{ww} is the power spectral density, α is the Kolmogorov constant equal to 1.56, k is the wavenumber, and n is the noise floor of the spectrum. Taylor's frozen turbulence hypothesis was employed to convert spectral frequencies into wavenumber space according to $k = 2\pi f/|\bar{u}|$. Only −5/3 slope lines with an R^2 goodness-of-fit greater than 0.8 were used in the analysis to ensure a well-defined inertial subrange and little contamination due to waves.

The highest ε levels were found at the dense site (Fig. 9), as was expected due to the substantially higher mean flow conditions. However, ε levels were smaller within the dense canopy, as compared to increased levels found within the sparse canopy, presumably due to the enhanced turbulence caused by flow interaction with the seagrass blades. Due to the more sparse geometry, the shear layer formed at the top of the canopy was thicker (Fig. 6), enabling a greater proportion of flow (relative to $\overline{u_0}$) to penetrate through the top of the canopy. This allowed for the production of both shear-layer and stem-generated turbulence (Nepf, 2012b) within the canopy, and contributed to the locally enhanced rates of ε. The bare site had ε levels similar to that of the sparse seagrass site, although with slightly reduced values at $z = 0.15$ m compared to $z = 0.35$ m.

3.5. Reynolds stress and momentum transport

Reynolds stress ($\overline{u'w'}$) estimates were computed for both wave-dominated and current-dominated flows from ADV measurements both above and within the canopy (Fig. 10). Although there is high variability in magnitude, measurements across the canopy-water interface showed a 20% decrease in the average Reynolds stress within the dense seagrass meadow (one-way ANOVA, $p = 0.05$). At the sparse site, average Reynolds stress within the canopy significantly increased by 70% (one-way ANOVA, $p < 0.05$), likely due to increased flow penetration of the more open canopy. The bare site showed a slight decrease in Reynolds stress at $z = 0.15$ m compared to higher in the water column at $z = 0.35$ m. Upper water column (above canopy) Reynolds stresses normalized by the square of the ambient velocity, $\overline{u'w'}/\overline{u_0^2}$, had values of $1.15 \pm 0.2 \times 10^{-2}$ for

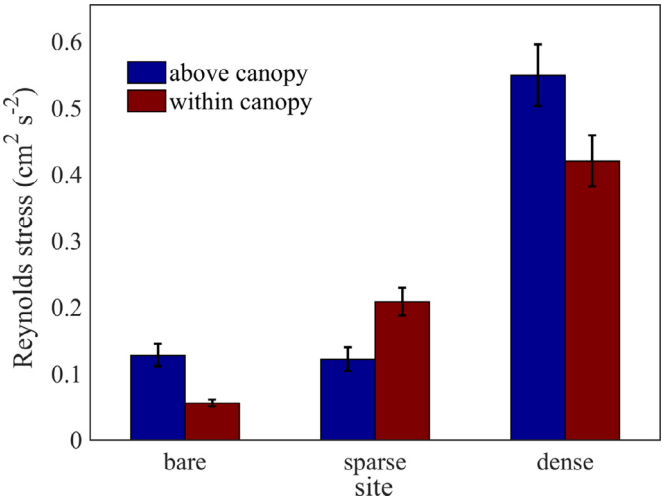

Fig. 10. Reynolds stress (±1 s.e.) at the bare, sparse, and dense seagrass sites.

the bare, $4.5 \pm 0.7 \times 10^{-2}$ for the sparse, and $1.6 \pm 0.2 \times 10^{-2}$ for the dense seagrass site.

To determine the mechanisms driving mixing across the canopy, a quadrant analysis (Lu and Willmarth, 1973) was performed, which describes the vertical transport of momentum due to correlated instantaneous motions in the horizontal and vertical directions. Quadrant analysis, since it is applied to instantaneous velocity motions, cannot be performed after wave-current decomposition; therefore, no wave dominated flows are presented. ADV data was first filtered to select for time periods both within and above the meadow with very little motion due to wave activity. The u' and w' values during these periods were then normalized by their standard deviations over a single 10 min averaging window before the full subset of samples was sorted into each of four quadrants. Quadrants 2 and 4 are responsible for the momentum transport through turbulent ejections (Q2), where low momentum fluid is fluxed upward into faster overlying flows, and sweeps (Q4), where high momentum fluid is fluxed downward toward the seafloor. Typically, momentum transport is dominated by these ejection and sweeping events, which advect low momentum fluid vertically upwards out of the meadow or transfer high momentum fluid vertically downward toward the seafloor.

Contours of the turbulent probability distribution function (pdf) are plotted, and the percent of the distribution in each quadrant is shown both within and above the canopy in Fig. 11 for current driven flow conditions. Above the canopy at the dense site, ejection (Q2) and sweeping (Q4) events account for 65% of the Reynolds stress. Within the canopy, this increases to 81%, with 44% of the motions caused by turbulent sweeps (Q4), suggesting that mixing across the seagrass canopy is enhanced by turbulent momentum transport near the canopy-water interface. At the sparse site, transport above the canopy was distributed evenly across Q2 and Q4, while within canopy motions were slightly dominated by turbulent ejections; Q1 (21%), Q2 (31%), Q3 (22%), Q4 (27%). Momentum transport was evenly distributed between Q2 and Q4 at the bare site (not shown).

The efficiency of turbulent momentum transport within the vertical direction can be determined by calculating a correlation coefficient for Reynolds stress ($\overline{u'w'}$) (Finnigan, 2000):

$$r_{uw} = \frac{\overline{u'w'}}{\sigma_u \sigma_w} \tag{7}$$

where σ_u and σ_w are the standard deviations of instantaneous horizontal (u) and vertical (w) velocities, respectively. Under wave forcing, the spectral wave-turbulence decomposition was first employed to remove oscillations in the horizontal and vertical velocity signal due to waves, and $\overline{u'w'}$ in Eq. (7) reflects only the Reynolds stress due to turbulence. The magnitude of the correlation coefficient indicates the degree of organization of the turbulence, with increasing magnitude reflecting more efficient momentum transport (Raupach et al., 1996). In vegetated layers, turbulent transport becomes more efficient through the modification of turbulence by the canopy that generates turbulent vortices. Overall, averages of $r_{uw} = -0.19$ for the sparse site, and $r_{uw} = -0.41$ for the dense site occurred under unidirectional flows. Values for unidirectional flows are comparable to published peak efficiencies of −0.32 for boundary layers and −0.44 for pure mixing layers (Ghisalberti and Nepf, 2002). Wave dominated flows showed a substantial reduction in mixing efficiency relative to unidirectional flow conditions. However, estimates of efficiency in momentum transport under wave forcing, as measured by Eq. (7), should be interpreted with caution since σ_u and σ_w are expected to be substantially higher and not a good predictor of levels of turbulence.

3.6. Fluid exchange and mass transport

During time periods surrounding dye tracer studies, average ambient velocities were 2.8 ± 1.0, 1.5 ± 0.9, and 3.2 ± 1.4 cm s^{-1} at the bare, sparse, and dense sites, respectively. Though ambient velocities were generally greater at the dense site, fluid retention was significantly greater within the meadow compared to the sparse site (one-way ANOVA with Bonferroni multicomparison, $p < 0.05$, Fig. 12). However, retention times were not statistically different between the three sites above the seagrass meadow (one-way ANOVA with Bonferroni multicomparison, $p = 0.1596$). Over the unvegetated seafloor, fluid retention was 2 times greater at $z = 0.15$ m than at $z = 0.35$ m. In comparison, the addition of seagrass structure enhanced the retention of fluids 4-fold within the canopy compared to above. Computed e-folding times ranged from 0.5–1.1 min (30–65 s) at measurement locations higher in the water column and 2–4.4 min (120–265 s) closer to the seafloor (Fig. 12). These values are in general agreement with other field studies on intertidal macroalgal canopies exposed to similar wave and turbulence environments, which found residence times of 5–37 s outside the canopy, and 18–142 s within the canopy (Nishihara et al., 2011).

4. Discussion

T. testudinum seagrass meadows were found to substantially lower mean currents adjacent to the seafloor compared to an unvegetated site. Reductions in velocity across the seagrass canopy were due to the development of fluid shear, which peaks at the top of the seagrass canopy (Lacy and Wyllie-Echeverria, 2011; Weitzman et al., 2015), and creates turbulence that controls the exchange of mass and momentum across the canopy-water interface (Nepf, 2012a). The thickness and magnitude of the shear layer control the degree of exchange across the canopy (Ghisalberti and Nepf, 2004), and the scale of penetration of turbulence into the canopy can be determined by:

$$\delta_e = \frac{0.23 \pm 0.06}{C_D a} \tag{8}$$

where C_D is the canopy drag, estimated as ~1 for submerged canopies (Nepf, 2012a), and a is the canopy frontal area per volume (Nepf et al., 2007). For the seagrass canopies in this study, this relationship predicts a penetration depth of ~ 2.6 cm at the sparse site and 1.0 cm at the dense site, suggesting greater exchange within the sparsely vegetated canopy. This is also in general agreement with the measured penetration of mean flows into the seagrass meadows (Fig. 6). Wave action was found to enhance flow penetration into the top of the seagrass canopy, especially within

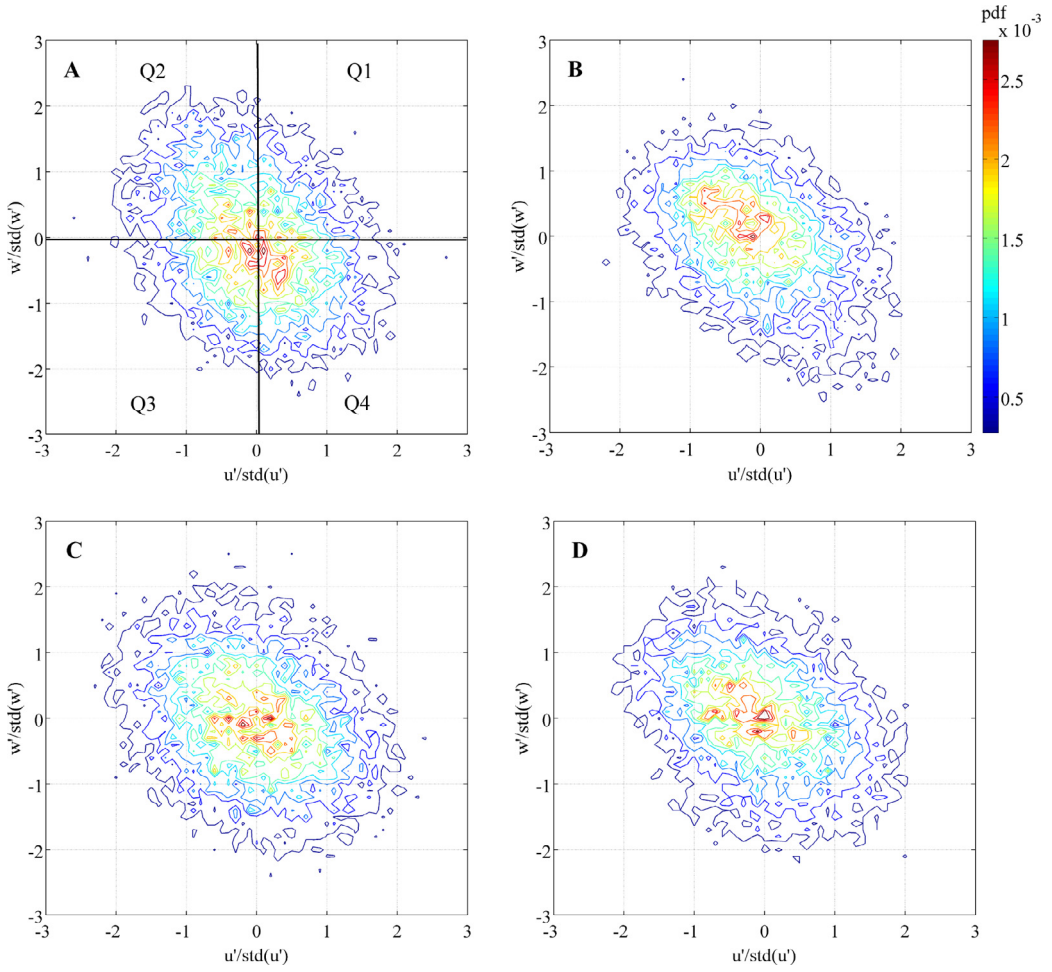

Fig. 11. Quadrant analysis of u' and w' turbulent fluctuations, normalized by their standard deviations (std) located **A** above and **B** within the seagrass bed at the dense site. Turbulent fluctuations **C** above and **D** within the seagrass bed at the sparse site.

the dense meadow. Although we were not able to quantify movement of the seagrass blades, the swaying of seagrass blades was observed under wave forcing within our PIV videos. The enhanced penetration depth within the seagrass may be caused by the oscillatory motion of the waves which periodically induced an opening and closing of the top of the canopy, thus enabling flow to be advected into the canopy.

Previous studies have found that oscillatory motion always enhances flow within a canopy (Lowe et al., 2005a), and in wave-dominated flows canopy drag does not influence oscillatory motion (Nepf, 2012a). The degree of reduction of oscillatory motion by the seagrass canopy can be predicted via the ratio of wave orbital excursion length (A) to blade spacing (ΔS), such that $A/\Delta S > 1$ indicates significant attenuation (Lowe et al., 2005a). The orbital excursion length was calculated as $A = u_{os}/\omega$, where u_{os} is the wave orbital velocity, and ω is the radian wave frequency ($\omega = 2\pi/T$, with the wave period (T) from directly above the canopy; Lowe et al., 2005a). For both density seagrass meadows $A/\Delta S < 1$, and therefore, orbital motion was expected to penetrate the seagrass canopy. While $A/\Delta S < 1$ for both canopies, the ratio was significantly greater at the dense than at the sparse site (one-way ANOVA, $p < 0.05$). As expected, for both the sparse and dense canopies, waves penetrated through the canopy and matched orbital motions predicted by linear wave theory. Further, wave-current flows containing both orbital and unidirectional velocities penetrated deeper into the sparse canopy, increasing rms velocities.

Under unidirectional currents, momentum transport in vegetated canopies is typically dominated by sweeping events (Finnigan, 2000) carrying high momentum fluid into the canopy from overlying flow. The prevalence of sweeping events over turbulent ejections increases with increasing canopy density (Finnigan, 2000). This was confirmed for the *T. testudinum* meadows, where at the sparse seagrass site turbulent sweeps accounted for just 27% of the Reynolds stresses, which increased to 44% within the dense seagrass meadow. Additionally, at the sparse canopy turbulent ejections accounted for a greater percentage of the momentum transport, where greater flow penetration also led to increased Reynolds stress below the canopy-water interface (relative to mean currents). This may have been caused by enhanced turbulence generated by local stem-wake interactions of the flow that more easily penetration into the sparse canopy (Ghisalberti and Nepf, 2004; Kondziolka and Nepf, 2014; Lawson et al., 2012). For both the sparse and dense canopies in this study, turbulence is dominated by canopy-generated vortices as $ah > 0.1$ (Nepf, 2012b). However, the relative depths of the canopies result in the sparse site being characterized as an unconfined canopy ($H/h > 10$) while the dense meadow is in the transition between unconfined and shallow submergence ($H/h \leq 5$, for the dense meadow $H/h = 7$) (Nepf, 2012b). With shallow submergence, canopy-scale vortices can dominant turbulence in the water column (Ghisalberti and Nepf, 2005). Conversely, at the sparse meadow canopy-scale vortices are stretched and secondary instabilities are more likely to occur

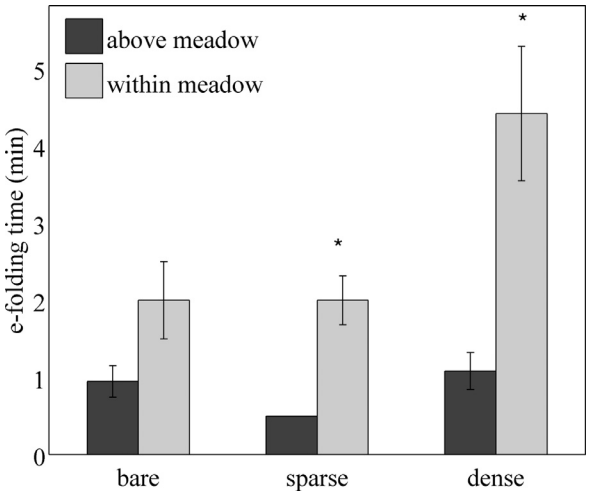

Fig. 12. Fluid retention represented with the *e*-folding time (±1 s.e.), which is the length of time for dye concentrations at a location to diminish to 1/e of the peak concentration. Concentration curves for Rhodamine WT dye were obtained at two vertical positions in the water column, equivalent to velocimeters' sampling volumes, at each of the three study sites (bare seafloor, sparse seagrass canopy, and dense seagrass canopy). * Denotes statistically significant difference between bars (one-way ANOVA with Bonferroni multicomparison, $p < 0.05$).

(Finnigan et al., 2009). These secondary instabilities could also lead to the increased turbulence observed at the sparse canopy.

Though greater turbulence was produced at the top of the canopy under wave conditions, results suggest turbulence due to waves may not be efficient at transporting momentum. The efficiency of turbulent momentum transport was quantified through a correlation coefficient for Reynolds stress, r_{uw}. Averages of r_{uw} ranged from −0.19 for unidirectional flows to −0.08 for wave-driven flows at the sparse site, and increased to $r_{uw} = -0.41$ and −0.09 for the dense site under unidirectional and wave dominated flows, respectively. However, it is expected that the variance in u and w will increase under oscillatory flow conditions, which would decrease overall efficiency of momentum transfer. Within a laboratory flume under unidirectional flows, Ghisalberti and Nepf (2006) did find a decrease in exchange efficiency and turbulent momentum transfer with oscillatory motion caused by the passing of turbulent vortices from monami waving of the seagrass canopy, which were smaller, weaker vortices than would be present in a rigid canopy. This may suggest that the movement of seagrass blades in a wavy environment acts to reduce the size and energy of turbulent vortices. Efficiency is generally greatest near the top of the canopy and decreases with depth into a vegetated canopy (Raupach et al., 1996; Shaw et al., 1974). Though the efficiency of the vertical momentum transport was low within the sparse meadow, both the Reynolds stress and turbulent dissipation was enhanced within the canopy. This increased the mixing across the canopy, as quantified by a reduction in *e*-folding time. This effect is presumably due to the enhanced turbulence caused by stem-wake interactions (Hansen and Reidenbach, 2013) and secondary instabilities generated by canopy-scale vortices of the unconfined sparse canopy (Finnigan et al., 2009).

Turbulence present within vegetated canopies increases exchange in the upper canopy (Nepf, 2012a), leading to enhanced exchange of scalars (such as nutrients and gases) across the canopy-water interface (Cornelisen and Thomas, 2004; Rheuban et al., 2014). For Florida Bay, as seagrass shoot density increased, the velocity shear generated at the top of the canopy increased (Fig. 6), however the turbulence generated did not penetrate deep into the canopy, thus reducing the vertical extent over which mixing occurred. In the presence of waves, the efficiency of momentum transport declined while the turbulence within both density canopies increased. Thus, the addition of waves enhances mixing across the canopy boundary, albeit at a less efficient rate as measured by Eq. (7). The enhanced fluid motion may not only increase the exchange of dissolved and particulate matter between the seagrass canopy and overlying water, but may also have the added effect of stimulating seagrass photosynthesis and respiration through the reduction in diffusive boundary layer thickness (Hume et al., 2011).

Acknowledgments

We thank Kate Walsh, Matt Long, Christine Romanowich, and Tom Frankovich for field study support, Joseph Zieman for logistical support, and Jacalyn Huband for data processing technical support. We also thank the Everglades National Park for granting permission to complete field studies within the park [permit number EVER-2009-SCI-0050] and the Key Largo Ranger Station for periodic lab space. This research was funded by an Everglades Foundation Research Fellowship to JCRH and a grant from the National Science Foundation [grant number NSF-OCE-1151314] to MAR.

References

Abdelrhman, M.A., 2002. Modeling how a hurricane barrier in New Bedford Harbor, Massachusetts, affects the hydrodynamics and residence times. Estuaries 25, 177–196.
Adams, M.P., Hovey, R.K., Hipsey, M.R., Bruce, L.C., Ghisalberti, M., Lowe, R.J., Gruber, R.K., Ruiz-Montoya, L., Maxwell, P.S., Callaghan, D.P., 2016. Feedback between sediment and light for seagrass: where is it important? Limnol. Oceanogr.
Adhitya, A., Bouma, T., Folkard, A., Van Katwijk, M., Callaghan, D., De Iongh, H., Herman, P., 2014. Comparison of the influence of patch-scale and meadow-scale characteristics on flow within seagrass meadows: a flume study. Mar. Ecol. Prog. Ser. 516, 49–59.
Benilov, A.Y., Filyushkin, B.N., 1970. Application of methods of linear filtration to an analysis of fluctuations in the surface layer of the sea. Itz. Atmos. Ocean. Phys. 6, 810–819.
Borum, J., Pedersen, O., Greve, T., Frankovich, T., Zieman, J., Fourqurean, J.W., Madden, C., 2005. The potential role of plant oxygen and sulphide dynamics in die-off events of the tropical seagrass, *Thalassia testudinum*. J. Ecol. 93, 148–158.
Bouma, T.J., Friedrichs, M., Klaassen, P., Van Wesenbeeck, B.K., Brun, F.G., Temmerman, S., Van Katwijk, M.M., Graf, G., Herman, P.M.J., 2009. Effects of shoot stiffness, shoot size and current velocity on scouring sediment from around seedlings and propagules. Mar. Ecol. Prog. Ser. 388, 293–297.
Bradley, K., Houser, C., 2009. Relative velocity of seagrass blades: Implications for wave attenuation in low-energy environments. J. Geophys. Res. Earth Surf. 114, 1–13.
Bricker, J.D., 2003. Bed Drag Coefficient Variability Under Wind Waves in a Tidal Estuary: Field Measurements and Numerical Modeling Ph.D. thesis. Stanford University, Stanford, CA.
Bricker, J.D., Monismith, S.G., 2007. Spectral wave-turbulence decomposition. J. Atmos. Ocean Technol. 24, 1479–1487.
Carr, J.A., D'odorico, P., Mcglathery, K.J., Wiberg, P.L., 2016. Spatially explicit feedbacks between seagrass meadow structure, sediment and light: habitat suitability for seagrass growth. Adv. Water Resour. 93, 315–325.
Cornelisen, C.D., Thomas, F.I., 2009. Prediction and validation of flow-dependent uptake of ammonium over a seagrass-hardbottom community in Florida Bay. Mar. Ecol. Prog. Ser. 386, 71–81.
Cornelisen, C.D., Thomas, F.I.M., 2004. Ammonium and nitrate uptake by leaves of the seagrass *Thalassia testudinum*: impact of hydrodynamic regime and epiphyte cover on uptake rates. J. Mar. Syst. 49, 177–194.
Cowen, E.A., Monismith, S.G., 1997. A hybrid digital particle tracking velocimetry technique. Exp. Fluids 22, 199–211.
Dean, R.G., Dalrymple, R.A., 1991. Water Wave Mechanics for Engineers and Scientists. World Scientific.
Finnigan, J., 2000. Turbulence in plant canopies. Annu. Rev. Fluid Mech. 32, 519–571.
Finnigan, J.J., Shaw, R.H., Patton, E.G., 2009. Turbulence structure above a vegetation canopy. J. Fluid Mech. 637, 387–424.
Fonseca, M.S., 1983. Comparisons of current flow and wave dynamics through four seagrass species. Estuaries 6.
Ghisalberti, M., Nepf, H.M., 2002. Mixing layers and coherent structures in vegetated aquatic flows. J. Geophys. Res. 107, 3-1–3-11.
Ghisalberti, M., Nepf, H.M., 2004. The limited growth of vegetated shear layers. Water Resour. Res. 40, W07502 07510.01029/02003WR002776.
Ghisalberti, M., Nepf, H.M., 2005. Mass transport in vegetated shear flows. Environ. Fluid Mech. 5, 527–551.
Ghisalberti, M., Nepf, H.M., 2006. The structure of the shear layer in flows over rigid and flexible canopies. Environ. Fluid Mechan. 6, 277–301.

Gross, T.F., Nowell, A.R., 1983. Mean flow and turbulence scaling in a tidal boundary layer. Cont. Shelf Res. 2, 109–126.
Hall, M.O., Durako, M.J., Fourqurean, J.W., Zieman, J.C., 1999. Decadal changes in seagrass distribution and abundance in Florida Bay. Estuaries 22, 445–459.
Hansen, J.C.R., Reidenbach, M.A., 2012. Wave and tidally driven flows in eelgrass beds and their effect on sediment suspension. Mar. Ecol. Prog. Ser. 448, 271–287.
Hansen, J.R., Reidenbach, M., 2013. Seasonal growth and senescence of a *Zostera marina* seagrass meadow alters wave-dominated flow and sediment suspension within a coastal bay. Estuar Coasts 1–16.
Holmquist, J.G., Powell, G.V., Sogard, S.M., 1989. Sediment, water level and water temperature characteristics of Florida Bay's grass-covered mud banks. Bull. Mar. Sci. 44, 348–364.
Hume, A.C., Berg, P., Mcglathery, K.J., 2011. Dissolved oxygen fluxes and ecosystem metabolism in an eelgrass (*Zostera marina*) meadow measured with the eddy correlation technique. Limnol. Oceanogr. 56, 86–96.
Koch, E., 1994. Hydrodynamics, diffusion-boundary layers and photosynthesis of the seagrasses *Thalassia testudinum* and *Cymodocea nodosa*. Mar. Biol. 118, 767–776.
Koch, E., 1999. Sediment resuspension in a shallow *Thalassia testudinum* banks ex Konig bed. Aquat. Bot. 65, 269–280.
Koch, E., Ackerman, J.D., Verduin, J., Van Keulen, M., 2006. Fluid dynamics in seagrass ecology-from molecules to ecosystems. In: Seagrasses: Biology, Ecology and Conservation. Springer Netherlands, pp. 193–225.
Koch, E., Gust, G., 1999. Water flow in tide- and wave-dominated beds of the seagrass *Thalassia testudinum*. Mar. Ecol. Prog. Ser. 184, 63–72.
Kondziolka, J.M., Nepf, H.M., 2014. Vegetation wakes and wake interaction shaping aquatic landscape evolution. Limnol. Oceanogr. 4, 106–119.
Lacy, J.R., Wyllie-Echeverria, S., 2011. The influence of current speed and vegetation density on flow structure in two macrotidal eelgrass canopies. Limnol. Oceanogr. 1, 38–55.
Lawson, S., Mcglathery, K., Wiberg, P., 2012. Enhancement of sediment suspension and nutrient flux by benthic macrophytes at low biomass. Mar. Ecol. Prog. Ser. 448, 259–270.
Lei, J., Nepf, H., 2016. Impact of current speed on mass flux to a model flexible seagrass blade. J. Geophys. Res. 121, 4763–4776.
Long, M.H., Berg, P., Falter, J.L., 2015. Seagrass metabolism across a productivity gradient using the eddy covariance, Eulerian control volume, and biomass addition techniques. J. Geophys. Res. 120, 3624–3639.
Lowe, R.J., Falter, J.L., Koseff, J.R., Monismith, S.G., Atkinson, M.J., 2007. Spectral wave flow attenuation within submerged canopies: implications for wave energy dissipation. J. Geophys. Res. 112 (C05018), 1–14. http://dx.doi.org/10.1029/2006JC003605.
Lowe, R.L., Koseff, J.R., Monismith, S.G., 2005a. Oscillatory flow through submerged canopies: 1. Velocity structure. J. Geophys. Res. 110. http://dx.doi.org/10.1029/2004JC002788.
Lowe, R.L., Koseff, J.R., Monismith, S.G., Falter, J.L., 2005b. Oscillatory flow through submerged canopies. Part 2. Canopy mass transfer. J. Geophys. Res. 110. http://dx.doi.org/10.1029/2004JC002789.
Lu, S.S., Willmarth, W.W., 1973. Measurements of the structure of the Reynolds stress in a turbulent boundary layer. J. Fluid Mech. 60, 481–571.
Luhar, M., Infantes, E., Orfila, A., Terrados, J., Nepf, H.M., 2013. Field observations of wave-induced streaming through a submerged seagrass (*Posidonia oceanica*) meadow. J. Geophys. Res. 118, 1955–1968.
Monsen, N.E., Cloern, J.E., Lucas, L.V., Monismith, S.G., 2002. A comment on the use of flushing time, residence time, and age as transport time scales. Limnol. Oceanogr. 47, 1545–1553.
Nepf, H.M., 2012a. Flow and transport in regions with aquatic vegetation. Annu. Rev. Fluid Mech. 44, 123–142.
Nepf, H.M., 2012b. Hydrodynamics of vegetated channels. J. Hydraul. Res. 50 (3), 262–279.
Nepf, H.M., Ghisalberti, M., White, B., Murphy, E., 2007. Retention time and dispersion associated with submerged aquatic canopies. Water Resour. Res. 43, W04422. http://dx.doi.org/10.1029/2006WR005362.
Nepf, H.M., Vivoni, E.R., 2000. Flow structure in depth-limited, vegetated flow. J. Geophys. Res. 105, 28547–28557.
Nishihara, G.N., Terada, R., Shimabukuro, H., 2011. Effects of wave energy on the residence times of a fluorescent tracer in the canopy of the intertidal marine macroalgae, *Sargassum fusiforme* (Phaeophyceae). Phycol. Res. 59, 24–33.
Peralta, G., Brun, F.G., Pérez-Lloréns, J.L., Bouma, T.J., 2006. Direct effects of current velocity on the growth, morphometry and architecture of seagrasses: a case study on *Zostera noltii*. Mar. Ecol. Prog. Ser. 327, 135–142.
Pujol, D., Serra, T., Colomer, J., Casamitjana, X., 2013. Flow structure in canopy models dominated by progressive waves. J. Hydrol. 486, 281–292.
Raffel, M., Willert, C.E., Kompenhans, J., 1998. Particle Image Velocimetry, A Practical Guide. Springer-Verlag.
Raupach, M., Finnigan, J., Brunet, Y., 1996. Coherent eddies and turbulence in vegetation canopies: the mixing-layer analogy. Boundary Layer Meteorol 60, 375–395.
Reidenbach, M.A., Monismith, S.G., Koseff, J.R., Yahel, G., Genin, A., 2006. Boundary layer turbulence and flow structure over a fringing coral reef. Limnol. Oceanogr. 51, 1956–1968.
Reidenbach, M.A., George, N.T., Koehl, M.A.R., 2008. Antennule morphology and flicking kinematics facilitate odor sampling by the spiny lobster, *Panulirus argus*. J. Exp. Biol. 211, 2849–2858.
Rheuban, J.E., Berg, P., Mcglathery, K.J., 2014. Ecosystem metabolism along a colonization gradient of eelgrass (*Zostera marina*) measured by eddy correlation. Limnol. Oceanogr. 59, 1376–1387.
Schanz, A., Asmus, H., 2003. Impact of hydrodynamics on development and morphology of intertidal seagrasses in the Wadden Sea. Mar. Ecol. Prog. Ser. 261, 123–134.
Shaw, R., Silversides, R., Thurtell, G., 1974. Some observations of turbulence and turbulent transport within and above plant canopies. Boundary Layer Meteorol. 5, 429–449.
Stocking, J.B., Rippe, J.P., Reidenbach, M.A., 2016. Structure and dynamics of turbulent boundary layer flow over healthy and algae-covered corals. Coral Reefs 35, 1047–1059.
Sveen, J.K., Cowen, E.A., 2004. Quantitative Imaging Techniques and Their Application to Wavy Flows. World Scientific Pub. Co.
Taylor, D., Nixon, S., Granger, S., Buckley, B., 1995. Nutrient limitation and the eutrophication of coastal lagoons. Mar. Ecol. Prog. Ser. 127, 235–244.
Thomas, F.I., Cornelisen, C.D., Zande, J.M., 2000. Effects of water velocity and canopy morphology on ammonium uptake by seagrass communities. Ecology 81, 2704–2713.
Trowbridge, J.H., 1998. On a technique for measurement of turbulent shear stress in the presence of surface waves. J. Atmos. Oceanic Technol. 15, 290–298.
Wang, J.D., Van De Kreeke, J., Krishnan, N., Smith, D., 1994. Wind and tide response in Florida Bay. Bull. Mar. Sci. 54, 579–601.
Weitzman, J., Aveni-Deforge, K., Koseff, J., Thomas, F., 2013. Uptake of dissolved inorganic nitrogen by shallow seagrass communities exposed to wave-driven unsteady flow. Mar. Ecol. Prog. Ser. 475, 65–83.
Weitzman, J.S., Zeller, R.B., Thomas, F.I., Koseff, J.R., 2015. The attenuation of current- and wave-driven flow within submerged multispecific vegetative canopies. Limnol. Oceanogr. 60, 1855–1874.
Wiberg, P.L., Sherwood, C.R., 2008. Calculating wave-generated bottom orbital velocities from surface-wave parameters. Computers Geosci 34, 1243–1262.
Widdows, J., Pope, N.D., Brinsley, M.D., Asmus, H., Asmus, R.M., 2008. Effects of seagrass beds (*Zostera noltii* and Z. marina) on near-bed hydrodynamics and sediment resuspension. Mar. Ecol. Prog. Ser. 358, 125–136.
Zieman, J., Fourqurean, J.W., Iverson, R.L., 1989. Distribution, abundance and productivity of seagrasses and macroalgae in Florida Bay. Bull. Mar. Sci. 44, 292–311.